THE GEOLOGICAL SOCIETY OF AMERICA®

# Characterizing seismites with anisotropy of magnetic susceptibility

T. Levi[1], R. Weinberger[1,2], G.I. Alsop[3] and S. Marco[4]
[1]Geological Survey of Israel, Jerusalem 95501, Israel
[2]Department of Geological and Environmental Sciences, Ben Gurion University of the Negev, Beer Sheva, Israel
[3]Department of Geology and Petroleum Geology, School of Geosciences, University of Aberdeen, Aberdeen AB24 3FX, UK
[4]Department of Geophysics, Tel Aviv University, Tel Aviv 69978, Israel

## ABSTRACT

**Characterizing seismites is a key factor in understanding earthquake kinematics, dynamics and resulting hazards. In order to understand the kinematics and dynamics of seismites, we analyzed the anisotropy of magnetic susceptibility (AMS) of various seismite types of known origin, which have formed during paleoseismic activity along the Dead Sea fault (DSF) system. The magnetic lineation (*L*) and the shape of the AMS ellipsoid (*T*) of the seismites are presented in a new *T* versus *L* plot. Depending on the type of material, the seismites are distinguished according to the following characteristics. Injection structures are characterized by a nonlinear correlation curve; co-seismic fault-related damage zones lie on a common linear correlation curve; earthquake-triggered folds also show a linear correlation with those that have undergone major deformation and have low *T* and high *L* values. Breccia layers display a range of *T* and *L* values similar to that of primary sedimentary layers, implying that such seismites were formed by material deposited immediately after an earthquake. This new application of AMS provides an effective tool for resolving the kinematics and dynamics of a wide variety of seismites in soft-sediments. We outline a robust procedure to infer the seismite mechanism, which is helpful in recovering paleoseismic records in complex settings.**

## INTRODUCTION

Earthquake-related seismites such as deformed sediments near co-seismic faults, folds, injection structures, breccia layers and fissures are important palaeoseismic indicators that promote the understanding of many aspects of tectonics (McCalpin, 1996). However, it is not always possible to identify seismites and often difficult to determine their mechanism of formation through direct field observations, in particular, where rocks are massive and do not exhibit distinct markers. We examine the possibility of detecting different seismite types through the analysis of anisotropy of magnetic susceptibility (AMS). The AMS analysis is generally used for characterizing petrofabrics in order to reveal flow directions and for quantifying weak inelastic deformation (e.g., Schwehr and Tauxe, 2003; Borradaile and Jackson, 2004). The AMS fabric is commonly represented as an ellipsoid, whose principal axes (eigenvectors), the maximum ($K_1$), intermediate ($K_2$), and minimum ($K_3$) magnetic susceptibility, correspond to $k_1$, $k_2$, and $k_3$ eigenvalues of the AMS. Because AMS analysis is one of the best techniques for identifying inelastic strain preserved in rocks (e.g., Borradaile and Jackson, 2004), it can also be applied to identify and characterize deformation in seismites (e.g., Levi et al., 2006a, 2006b). However, attempts to correlate seismites with different processes based solely on projecting the AMS axes might lead to incorrect interpretations. On the other hand, the AMS parameters that represent the magnitude and the shape of the AMS ellipsoid may be useful in identifying different seismites. For example, it is well known that the magnetic lineations, $L = k_1/k_2$, begin to develop during progressive deformation, preserving the strain stored in the rocks (e.g., Parés and van der Pluijm, 2002) and the shape of the AMS ellipsoid (Jelinek, 1981) (*T*) can be correlated with the strain magnitude and its history of deformation (e.g., Parés and van der Pluijm, 2003). Magnetic lineation, foliation, and the shape of the AMS may reflect magnetic fabrics forming differently as a result of the deposition, transport, and deformation of rocks (Borradaile and Jackson, 2004). AMS has also been correlated with strain in rocks and the tectonic deformation of sediments (Levi and Weinberger, 2011), and has been used to characterize soft-sediment deformation (Schwehr and Tauxe, 2003; Weinberger et al., 2017; Issachar et al., 2015).

Despite the importance of characterizing seismites, no previous attempt has apparently been made to examine whether different seismites can be separated and characterized by AMS parameters. We therefore aim to relate seismites to characteristic processes by analyzing the AMS parameters of a range of recent (<40 k.y.) seismite types that formed in association with paleoseismic activity along the Dead Sea fault (DSF) system (Fig. 1). In this study, we pursue the idea that various seismite types in soft sediments can be detected through the use of *L* and *T* parameters.

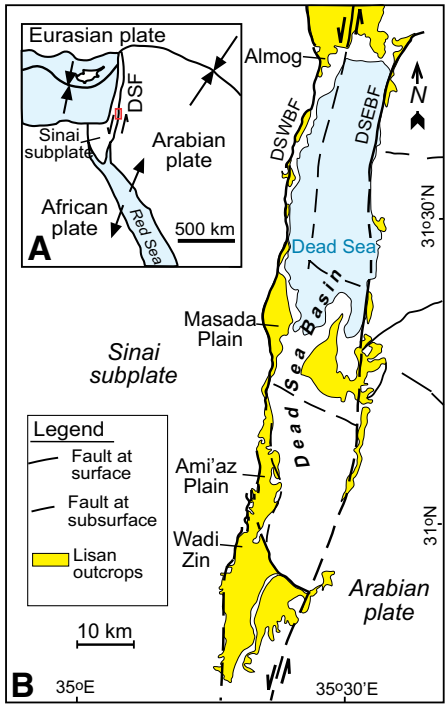


**Figure 1. A: General tectonic map showing the location of the study area (small red box) along the Dead Sea fault (DSF) system. B: Map of the Dead Sea Basin showing outcrops of the Lisan Formation and the position of strands of the DSF system (Sneh and Weinberger, 2014); dashed line is subsurface fault. DSWBF—Dead Sea Western Border Fault zone; DSEBF—Dead Sea Eastern Border Fault.**

## GEOLOGIC SETTING

The DSF system is one of the most active tectonic features in the Middle East, and comprises several tectonic depressions, the most prominent of which is the Dead Sea Basin (DSB) (Fig. 1; Garfunkel et al., 2014, and references therein). The Lisan Formation was deposited in the DSB between 70 and 15 ka (Haase-Schramm et al., 2004) and exposes numerous seismities (Marco and Agnon, 2005; Levi et al., 2006a, 2006b; Alsop and Marco., 2012; Weinberger et al., 2017) that are the focus of the present study. The lacustrine sediments of the Lisan Formation comprise an ~40 m sequence of alternating white authigenic aragonite and fine, dark detrital laminae.

Paleoseismic records reveal numerous M > 5.5–6 earthquake events, as well as several M > 7 earthquake events, during the late Pleistocene and the Holocene (Marco and Klinger, 2014). During this seismic activity, different types of seismites were formed (Fig. 2): (1) a set of syn-depositional normal faults and an envelope of deformed rock volume, known as a damage zone (Levi et al., 2014); (2) folds and fold-thrust systems, which formed mass transport deposits (MTDs) at the near surface that were controlled by gravity-driven movement toward the depocenter (Alsop and Marco, 2012; Alsop et al., 2017; Weinberger et al., 2017); (3) injection clastic dikes, which formed due to fluidization of the Lisan source layers during seismic events (Levi et al., 2006a, 2006b); (4) sheared clastic dikes, which are associated with coseismic horizontal bedding-plane slip and gouge formation (Weinberger et al., 2016); and (5) breccia layers, which formed on the bottom of the lake by the mixing of laminated fragments in Dead Sea water during earthquake shaking (Marco and Agnon, 2005). Following significant drying of Lake Lisan at 14–11 ka, and the occurrence of strong earthquakes, sets of clastic dikes were formed dynamically by host-rock fracturing and injection of the fluidized detrital material from the source layers (Levi et al., 2006a, 2006b). The injection of this fluidized material ~18 m below the surface was mainly vertical, in association with turbulent flow conditions, while close to the surface, the injection was horizontal and laminar (Levi et al., 2006b).

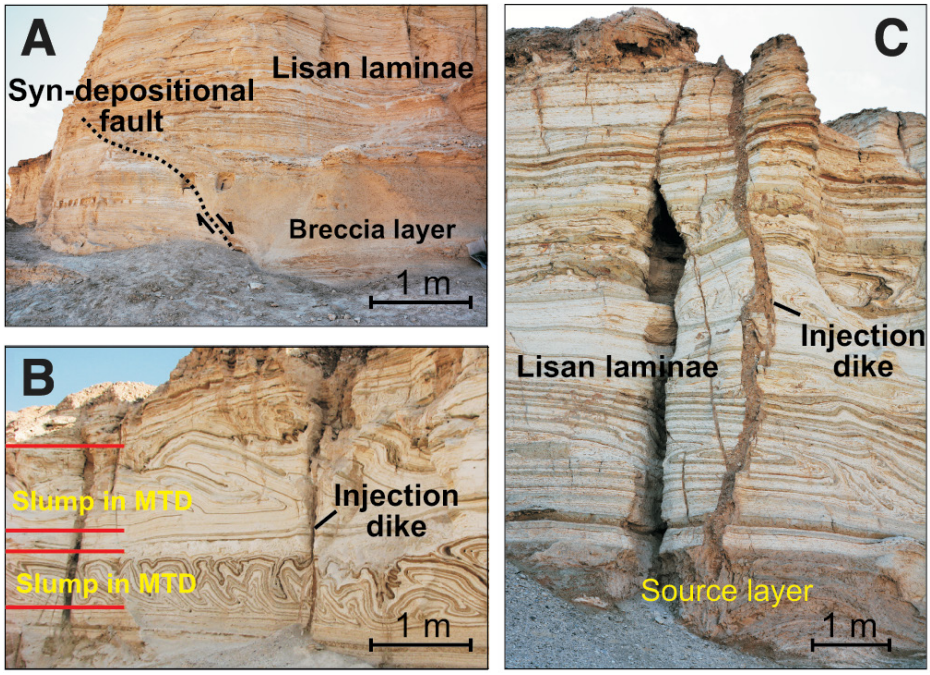


**Figure 2. A: A normal fault in the Masada Plain with a breccia layer located at the hanging wall on the right. B: Two sets of mass transport deposits (MTD) in Ami'az Plain, cross-cut by an injection clastic dike. C: An injection clastic dike in Ami'az Plain filled with clay-rich sediment, cross-cutting the Lisan Formation ~12 m above its source layer.**

## THE *T-L* PLOT

AMS may be represented by a magnitude ellipsoid, where the most frequently used anisotropy parameters are the mean susceptibility $k_m$, the anisotropy degree $P$, the magnetic lineation $L$, the magnetic foliation $F$, and the AMS shape parameter $T$, measuring the range from prolate ($-1 < T < 0$) through neutral ($T = 0$) to oblate ($0 < T < 1$) ellipsoids (Jelinek, 1981; Borradaile and Jackson, 2004).

During deformation of soft sediments, the strain ellipsoid may vary and be accompanied by formation of a lineation. Respectively, this process can be expressed as an increase in the values of $L$ and a change in the value of $T$. However, the use of such plots, or similar, has not yet been implemented (but see the *T-F* relations of Hrouda and Ježek [2014, their equation 12]), especially in the study of soft-sediment deformation.

Mathematically, $L$ is described as:

$$L = P\left(k_3 / k_2\right), \quad (1)$$

where

$$P = \left(k_1 / k_3\right) \quad (2)$$

is the anisotropy degree. The AMS shape parameter $T$ (Jelinek, 1981) is described as

$$T = \left(2\ \ln k_2 - \ln k_1 - \ln k_3\right) / \left(\ln k_1 - \ln k_3\right). \quad (3)$$

Equation 1 can be presented according to the log rules

$$\ln(L) = \ln\left(\frac{k_1}{k_3}\right) + \ln\left(\frac{k_3}{k_2}\right). \quad (4)$$

Inserting Equation 4 into Equation 3, the *T-L* can be then described as

$$T = \left[-\frac{2}{\ln\left(\frac{k_1}{k_3}\right)}\ln(L)\right] + 1, \quad (5)$$

where a line is defined with slope of $-\frac{2}{\ln\left(\frac{k_1}{k_3}\right)}$ and an intercept of 1.

For convenience, ln($L$) can be approximated as $L - 1$ (within 5% for values ranging between 1 and ~1.1), or the $L$ values can be presented on a logarithmic axis.

In cases where the samples share similar $k_1/k_3$, the slope of Equation 5 is expected to be constant and the correlation between $T$ and $L$ is linear (up to $L \approx 1.2$) (Fig. 3; A curve). For these samples, the results are displayed in the lower-left half of the plot, below the line corresponding to the sample with the maximum $P$. In cases where the samples do not share similar $k_1/k_3$, the correlation between $T$ and $L$ is expected to be nonlinear (Fig. 3; B curve). On the basis of the underlying significance of the AMS parameters described here, we hypothesize that different types of seismites are diagnosed differently in the *T-L* plot.

## MAGNETIC FABRICS OF THE LISAN SEISMITES

The white aragonite of the Lisan Formation consists mainly of diamagnetic aragonite, while the brownish-green detritus layers have positive bulk AMS susceptibility. Titanomagnetite and

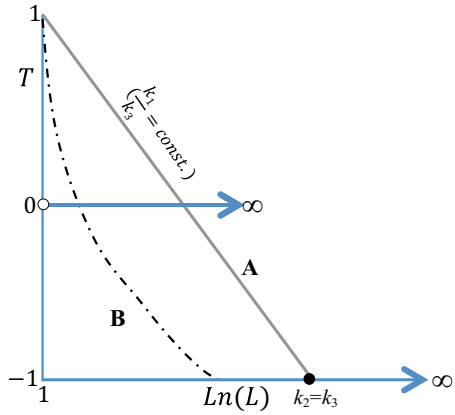


**Figure 3. Plot of the shape of the anisotropy of magnetic susceptibility (AMS) ellipsoid (*T*) versus magnetic lination (*L*). Gray and the dashed lines represent two possible types of correlation curves: (1) linear marked by "A" and (2) nonlinear marked by "B". White dot indicates an undefined value $T = 0$. Black dot indicates $T = -1$ where eigenvalues $k_2 = k_3$. Note that when $T = -1$ then $L = P$ (the anisotropy degree), and when $T$ approaches 1, $L = 1$ and $P$ is unconstrained.**

magnetite are the main ferromagnetic carriers in the detrital laminae (e.g., Levi et al., 2006a, 2006b, 2014).

We analyzed 588 samples of different seismite types, located in sites that are spread along ~80 km of one of the main segments of the DSB (Fig. 1A; Table DR1 in the GSA Data Repository[1]). Two outcrops consisting of undisturbed beds act as reference layers, and are made up of alternating white aragonite and brownish-green detritus from the Ami'az Plain (Fig. 1B). In order to test the effect of strain along the folded layers, and the effect of the material properties on the AMS parameters, the *T* and *L* values are presented in two *T*-*L* plots: (1) seismites formed of alternating aragonite-detritus laminae; and (2) seismites formed solely of detritus. Detailed AMS analysis was carried out along the folded layers.

## RESULTS

Figure 4A shows the *T*-*L* plot [i.e., ln(*L*) values are displayed along the *x* axis] of seismites composed of aragonite layers. The correlation obtained in this plot was linear and relatively high. Based on the seismite types, three main groups were obtained along the same correlation curve. Group A ranges from $T = 0.61$ up to $T = 0.98$ and $L = 1$ up to $L = 1.002$, and includes the reference layer, breccia layers, and sedimentary layers near the faults. Group B ranges from $T = 0.3$ up to $T = 0.76$ and $L = 1.004$ up to $L = 1.014$, and includes damage zones and gouges. Group C ranges from $T = –0.16$ up to $T = 0.6$ and $L = 1.004$ up to $L = 1.022$, and includes folds. Detailed analysis of the folds shows that the values of *L* and *T* are arranged along the correlation curve, depending on the structural domains within the fold itself (Tables DR2 and DR3).

The *T*-*L* plot of folded layers and clastic dikes formed of injected detritus (Fig. 4B) shows that the correlation obtained for the folds (Group D) is linear and relatively high, whereas that obtained for the vertical and horizontal injections (Group E) are nonlinear and relatively low and high, respectively. The folded detrital layers are similar to the aragonite layers, in that their horizontal layers have high *T* and low *L* values. On the other hand, vertical layers in the forelimbs have low *T* and high *L* values (Tables DR2 and DR3). In clastic dikes where the material was injected horizontally, the values of *T* are high and the values of *L* are low, whereas in vertical and turbulent injections the values of *T* are low and the values of *L* are intermediate to high.

## DISCUSSION AND CONCLUSIONS

In order to relate magnetic fabrics of sedimentary rocks with different deformation processes, it is beneficial to look at data sets in different ways, since all the bi-parametric plots such as *L*-*F* (Parés and van der Pluijm, 2002, 2003;), $P - k_m$ (e.g., Ferré et al., 2014), and *T*-*P* (e.g., Cifelli et al., 2009) quantify some aspect of the magnetic ellipsoid shape. It is noteworthy that none of the above-mentioned plots have been tested for a large variety of seismites (Fig. DR1). In addition to the common bi-parametric plots, it is shown that for a certain type of material, the *T*-*L* plot allows seismites of different origins to be correlated with specific types of deformation. Accordingly, the *T*-*L* plot shows that seismite types are organized into five main groups.

Group A (Fig. 4A), including sedimentary layers near a fault and breccia layers, is characterized by high *T* and low *L* values. The values *T* and *L* (site average) of the breccia layers reflects the suspension and the re-deposition processes that occurred during earthquake events over the lake floor. The 'sedimentary' *T* and *L* values characterizing these layers is evidence of these processes (Fig. 4A; Fig. DR2b). In some cases, the flow above the hangingwall was to the west (Figs. DR2b and DR2c), opposite to the direction of the regional transport that is expected to move eastward toward the depocenter of the basin (Alsop and Marco, 2012; Weinberger et al., 2017). It is reasonable to assume that those processes could have lasted hours or even several days after the event.

Group B (Fig. 4A), including the damage zones, gouges (polygon #B), and Group C of folds (polygon #C), are characterized by a linear trend extending to low *T* and high *L* values. During the faulting, the damage zones and the gouges were associated with an inelastic deformation (Levi et al., 2014). This deformation is expressed by the formation of a magnetic lineation and a decrease in oblateness, as identified by the negative linear correlation curve reaching to $L = 1.014$ and $T = 0.3$ (Fig. 4A). It was previously demonstrated that the formation of this magnetic fabric did not take more than a few seconds (Levi et al., 2014). The strain magnitude of the folds, indicating a significant shortening, is likely to be higher than that of the damage zones. Indeed, in the *T*-*L* plot, the folds have high *L* values (up to 1.023) and low *T* values (up to –0.4). *L* and *T* values of several structural domains of the folds (i.e., forelimbs, hinges) are located at the extreme end of the *T*-*L* curve or at the overlapping zone with Group B (Fig. 4A; Fig. DR3a). This indicates that the deformation along the folded layers is heterogeneous (e.g., Weinberger et al., 2017).

Group D includes folded detritus layers and injection clastic dikes (Group E) infilled by detrital material (Fig. 4B). Figure 4B shows that the *T*-*L* trend is linear, with a steeper slope than that of the aragonite layers, consistent with a smaller value of *P*. The original *P* of the aragonite reference layer is higher (1.028) than that of the detrital reference layer (1.016).

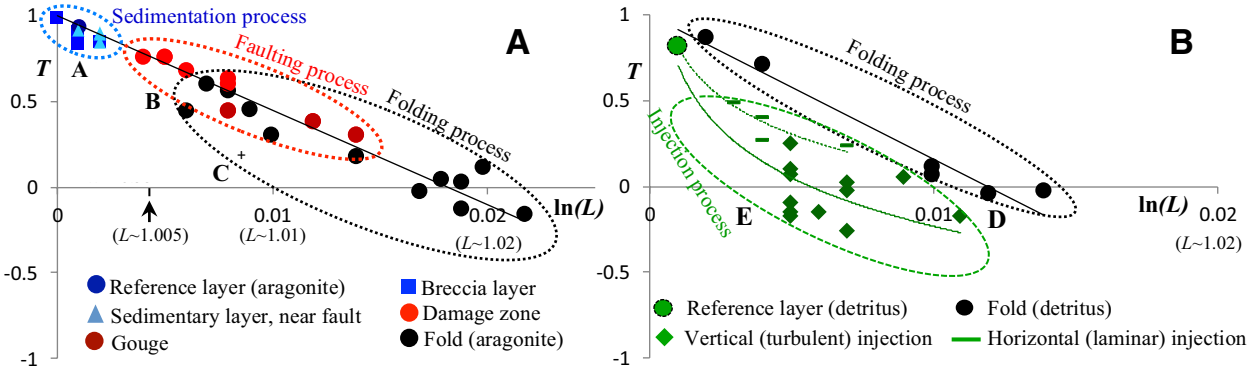


**Figure 4. A: Plot of the shape of the anisotropy of magnetic susceptibility (AMS) ellipsoid (*T*) versus magnetic lination (*L*) for different seismite types containing aragonite material. Black line marks the linear correlation curve ($y = –55x + 1$; $R^2 = 0.95$). B: *T*-*L* plot of different seismite types containing detrital material. Black line marks the linear correlation curve of the folds ($y = –84x + 1$; $R^2 = 0.96$), and the green solid and dashed lines mark the nonlinear correlation curves of the vertical ($y = –0.4 \ln x – 2$; $R^2 = 0.68$) and the horizontal ($y = –0.3\ln x – 1.4$; $R^2 = 0.94$) injections, respectively.**

[1]GSA Data Repository item 2018308, Tables DR1–DR3 (AMS data), Figure DR1 (common biparametric plots), Figure DR2 (AMS fabrics), and Figure DR3 (*T*-*L* plot of folds), is available online at http://www.geosociety.org/datarepository/2018/, or on request from editing@geosociety.org.

This anisotropy difference may be related to the crystallographic structure of the aragonite needles, whose alignment causes a high anisotropy (Hrouda, 2004) compared to that of the clay and ferromagnetic minerals of the detrital layers. This difference may also be sustained during the fracturing and folding, which is confirmed by the *T-L* plot, showing that the greater the $k_1/k_3$ the lower the slope (absolute value) of a given material (Equation 5; Fig. 4A).

Unlike other seismite types, during the injection process the particles completely lose their cohesion and mobilize away from the source layer; and because the shear rate may change from place to place, the sites no longer share a common $k_1/k_3$. Under these conditions, the oblate shape of the magnetic fabric decreases (Levi et al., 2006a, 2006b), and the lineation is relatively low. Figure 4B shows that the range of *L* and *T* values of the clastic dikes is almost fully distinguishable from the range of values of the folds, although both types of seismites are formed of the same detrital material. It is likely that the variations between the flow types (Fig. 4B) are related to the differences between turbulent (fast flow) and laminar flow (slow flow) conditions (Levi et al., 2006a, 2006b, and references therein).

The type of material has a significant effect on the initial values and evolution of *T* and *L* parameters, and hence, the seismite AMS data should first be displayed in accordance with the type of material (Figs. 4A and 4B). In cases where the correlation curve is nonlinear, then the seismite can be attributed to fluidization. Conversely, if the correlation curve is linear, then the seismite can be attributed to folding, development of a fault-related damage zone, and deposition. Further, if the sites have low *T* and high *L* values (Figs. 4A and 4B, Groups C and D) then the seismites can be attributed to folding accompanied by high strain. In cases where the sites are located near faults and have a range of *T-L* values similar to that of Group B (Fig. 4A), then the tested layers may be related to the development of damage zones. If the tested layers are located close to the fault and have a range of *T-L* values similar to that of Group A (Fig. 4A), it can be assumed that these layers did not undergo significant deformation. In cases where the seismites are breccia layers and have a range of *T-L* values similar to that of Group A, it can be assumed that these layers did not undergo any kind of deformation other than re-deposition. The re-deposition occurred over the lake floor immediately after the earthquakes, and is different from damage zones that were developed near coseismic faults; this can help to estimate the width of the damage zone and, hence, the total displacement along the coseismic fault. In cases where the range of *T-L* values differs from that of Group A and others, it can be assumed that additional processes occurred during or after the seismite formation.

This study shows that, in addition to the common bi-parametric plots, a *T-L* plot can help to distinguish between the kinematics by which different seismites were formed in soft sediments. It may therefore prove helpful in recovering paleoseismic records in complex geological settings, and in studying deformation such as folding and fault-related damage zones in other tectonic environments.


## ACKNOWLEDGMENTS

This study was supported by grants from the Israeli Government under Geological Survey of Israel DS project 40706, and the Israel Science Foundation (ISF grants 868/17). We are indebted to Vladimir Lyakhovsky for helpful discussions during the course of this study, and to Mike Jackson, Bjarne Almqvist, and Jason Patton for providing constructive and very helpful reviews.


## REFERENCES CITED


Alsop, G.I., and Marco, S., 2012, A large-scale radial pattern of seismogenic slumping towards the Dead Sea Basin: Journal of the Geological Society, v. 169, p. 99–110, https://doi.org/10.1144/0016-76492011-032.

Alsop, G.I., Marco, S., Levi, T., and Weinberger, R., 2017, Fold and thrust systems in Mass Transport Deposits: Journal of Structural Geology, v. 94, p. 98–115, https://doi.org/10.1016/j.jsg.2016.11.008.

Borradaile, G.J., and Jackson, M., 2004, Anisotropy of magnetic susceptibility (AMS): Magnetic petrofabrics of deformed rocks, *in* Martín-Hernández, F., et al., eds., Magnetic Fabric: Methods and Applications: Geological Society of London Special Publications, v. 238, p. 299–360, https://doi.org/10.1144/GSL.SP.2004.238.01.18.

Cifelli, F., Mattei, M., Chadima, M., Lenser, S., and Hirt, A.M., 2009, The magnetic fabric in "undeformed clays": AMS and neutron texture analyses from the Rif Chain (Morocco): Tectonophysics, v. 466, p. 79–88, https://doi.org/10.1016/j.tecto.2008.08.008.

Ferré, E.C., Gébelin, A., Till, J.L., Sassier, C., and Burmeister, K.C., 2014, Deformation and magnetic fabrics in ductile shear zones: A review: Tectonophysics, v. 629, p. 179–188, https://doi.org/10.1016/j.tecto.2014.04.008.

Garfunkel, Z., Ben-Avraham, Z., and Kagan, E., eds., 2014, Dead Sea Transform Fault System: Reviews: Dordrecht, Springer, 359 p.

Haase-Schramm, A., Goldstein, S.L., and Stein, M., 2004, U-Th dating of Lake Lisan aragonite (late Pleistocene Dead Sea) and implications for glacial East Mediterranean climate change: Geochimica et Cosmochimica Acta, v. 68, p. 985–1005, https://doi.org/10.1016/j.gca.2003.07.016.

Hrouda, F., 2004, Problems in interpreting AMS parameters in diamagnetic rocks, *in* Martín-Hernández, F., et al., eds., Magnetic Fabric: Methods and Applications: Geological Society of London Special Publications, v. 238, p. 49–59.

Hrouda, F., and Ježek, J., 2014, Frequency-dependent AMS of rocks: A tool for the investigation of the fabric of ultrafine magnetic particles: Tectonophysics, v. 629, p. 27–38, https://doi.org/10.1016/j.tecto.2014.01.040.

Issachar, R., Levi, T., Marco, S., and Weinberger, R., 2015, Anisotropy of magnetic susceptibility in diamagnetic limestones reveals deflection of the strain field near the Dead Sea Fault, northern Israel: Tectonophysics, v. 656, p. 175–189, https://doi.org/10.1016/j.tecto.2015.06.021.

Jelinek, V., 1981, Characterization of magnetic fabric of rocks: Tectonophysics, v. 79, p. 63–67, https://doi.org/10.1016/0040-1951(81)90110-4.

Levi, T., Weinberger, R., Aïfa, T., Eyal, Y., and Marco, S., 2006a, Earthquake-induced clastic dikes detected by anisotropy of magnetic susceptibility: Geology, v. 34, p. 69–72, https://doi.org/10.1130/G22001.1.

Levi, T., Weinberger, R., Aïfa, T., Eyal, Y., and Marco, S., 2006b, Injection mechanism of clay-rich sediments into dikes during earthquakes: Geochemistry Geophysics Geosystems, v. 7, https://doi.org/10.1029/2006GC001410.

Levi, T., and Weinberger, R., 2011, Magnetic fabrics of diamagnetic rocks and the strain field associated with the Dead Sea fault, northern Israel: Journal of Structural Geology, v. 33, p. 566–578, https://doi.org/10.1016/j.jsg.2011.02.001.

Levi, T., Weinberger, R., and Marco, S., 2014, Magnetic fabrics induced by dynamic faulting reveal damage zone sizes in soft rocks, Dead Sea basin: Geophysical Journal International, v. 199, p. 1214–1229, https://doi.org/10.1093/gji/ggu300.

Marco, S., and Agnon, A., 2005, High-resolution stratigraphy reveals repeated earthquake faulting in the Masada Fault Zone, Dead Sea Transform: Tectonophysics, v. 408, p. 101–112, https://doi.org/10.1016/j.tecto.2005.05.036.

Marco, S., and Klinger, Y., 2014, Review of on-fault palaeoseismic studies along the Dead Sea Fault, *in* Garfunkel, Z., et al., eds., Dead Sea Transform Fault System: Reviews: Modern Approaches in Solid Earth Sciences, v. 6, p. 183–205, https://doi.org/10.1007/978-94-017-8872-4_7.

McCalpin, J.P., ed., 1996, Paleoseismology: San Diego, Academic Press, International Geophysical Series, v. 62, 588 p.

Parés, J.M., and van der Pluijm, B.A., 2002, Evaluating magnetic lineations (AMS) in deformed rocks: Tectonophysics, v. 350, p. 283–298, https://doi.org/10.1016/S0040-1951(02)00119-1.

Parés, J.M., and van der Pluijm, B.A., 2003, Magnetic fabrics and strain in pencil structures of the Knobs Formation, Valley and Ridge Province, US Appalachians: Journal of Structural Geology, v. 25, p. 1349–1358, https://doi.org/10.1016/S0191-8141(02)00197-9.

Schwehr, K., and Tauxe, L., 2003, Characterization of soft-sediment deformation: Detection of cryptoslumps using magnetic methods: Geology, v. 31, p. 203–206, https://doi.org/10.1130/0091-7613(2003)031<0203:COSSDD>2.0.CO;2.

Sneh, A., and Weinberger, R., 2014. Major Structures of Israel and Environs: Jerusalem, Israel Geological Survey, scale 1:50,000.

Weinberger, R., Levi, T., Alsop, G.I., and Eyal, Y., 2016, Coseismic horizontal slip revealed by sheared clastic dikes in the Dead Sea Basin: Geological Society of America Bulletin, v. 128, p. 1193–1206, https://doi.org/10.1130/B31415.1.

Weinberger, R., Levi, T., Alsop, G.I., and Marco, S., 2017, Kinematics of Mass Transport Deposits revealed by magnetic fabrics: Geophysical Research Letters, v. 44, p. 7743–7749, https://doi.org/10.1002/2017GL074471.



Manuscript received 8 May 2018
Revised manuscript received 24 July 2018
Manuscript accepted 27 July 2018

Printed in USA